The Role of the Hubble parameter in Galactic Rotation Curves and Spiral Morphology

E.P.J. de Haas[1, a)]

Kandinsky College, Nijmegen, The Netherlands

We investigate the influence of the Hubble parameter $H(z)$ on galactic dynamics and morphology. By introducing the cosmic expansion as an effective limit on Newtonian gravitation, we obtain a redshift-dependent critical radius that constrains both spiral structure and rotation curves. Galactic bars are interpreted as frozen spirals of high-z epochs nested inside extended low-z spirals. This framework naturally explains the coexistence of bulges, bars, disks and halos as the outcome of metric inflow and bulge reset events. The resulting morphology and kinematics provide a direct and testable connection between galactic structure and the cosmic expansion. We argue that this approach opens a new possibility to empirically derive $H(z)$ from galaxy morphology and rotation curves and allows reconstructing the expansion history of the universe on galactic scales.

Keywords: alternative gravity theory, quantum gravity, space quantisation, Dark Matter, Dark Energie, Hubble expansion

[a)]Electronic mail: haas2u@gmail.com

I. INTRODUCTION

In this paper we combine the idea of galactic dynamics as presented in [1; 2] with the principle that the Hubble expansion puts an effective limit on the reach of Newtonian gravitation, as presented in [3]. We develop the idea that the Hubble parameter $H(z)$ fundamentally influences galactic dynamics and morphology throughout the different epochs of the cosmos. Galactic spirals contain a frozen memory of cosmic epochs through the constraint of the time dependent Hubble expansion on the Newtonian gravitational potential. The critical distance, in its time dependent form with $H(z)$ instead of H_0, tightens galactic spirals and reduces their extent in space. This idea, first presented in [3], automatically applies to galactic rotation curves as well. The dependence of galactic rotation curves on the Hubble parameter $H(z)$ is as significant than the dependence of the spirals, because those rotation curves are easier quantifiable than the exact form of the galactic spirals. One of the new ideas presented in this paper is that galactic bars in spiral disk galaxies are themselves spirals: time-frozen high-z compact spirals nested in lower-z large spirals. This approach opens the possibility to empirically derive the Hubble parameter from galaxy morphology and rotation curves, independent of standard cosmological assumptions, and to reconstruct $H(z)$ across a broad redshift range.

But we start the paper with the derivation of the correct metric velocities $\vec{v}_{rad,eff} = v_{rad,eff}\hat{r}$, $\vec{v}_{orb} = v_{orb}\hat{\varphi}$ and $\vec{v}_L = \vec{v}_{orb} + \vec{v}_{rad,eff}$, and the correct spiral pitch angle $tan(\alpha) = \frac{v_{rad,eff}}{v_{orb}}$, as corrected for the Hubble expansion influence. Our spiral pitch angle α is r dependent. It has no relation at all with the spiral pitch angle used in the literature that is obtained through a logarithmic function and has one single value for the entire spiral. The logarithmic pitch angle used in standard geometric spiral fitting is a purely geometric product, while ours is derived from galactic dynamics due to its r, R, M and Hz dependence.

II. EXTRACTING $H(z)$ FROM GALACTIC ROTATION CURVES.

This setion builds on the papers [1; 2], were we presented the constant Lagrangian postulate for galactic rotation curves and spirals. In this section we replace the Newtonian potential in this constant Lagrangian postulate by the effective radial Newtonian potential, understood as the Newtonian radial potential metric inflow minus the Hubble expansion metric outflow, as seen from the perspective of a central mass M. We start by deriving the effective radial potential and then

apply this to adjust the constant Lagrangian postulate's formulas.

A. Effective Potential for $r \leq R$, the bulge

We start from the classical potential per unit mass inside a uniform-density bulge and want to adjust this for the Hubble expansion putting a limit to the effective Newtonian reach:

$$\frac{V(r)}{m} = -\frac{GM}{2R}\left(3 - \frac{r^2}{R^2}\right)$$

First we convert this to a radial inflow velocity of the metric, using the escape kinetic energy equivalence:

$$\frac{1}{2}v_{\text{rad}}^2(r) = -\frac{V(r)}{m} \quad \Rightarrow \quad v_{\text{rad}}(r) = \sqrt{\frac{2GM}{2R}\left(3 - \frac{r^2}{R^2}\right)} = \sqrt{\frac{GM}{R}\left(3 - \frac{r^2}{R^2}\right)}$$

We then subtract the Hubble expansion velocity, which is a metric effect too, and define the effective intrinsic radial velocity of space as

$$v_{\text{rad,eff}}(r, Hz) = v_{\text{rad}}(r) - v_{Hz} = v_{\text{rad}}(r) - H_z r.$$

We then convert this back to a modified potential energy and call the result the effective Newtonian potential, as corrected for the Hubble expansion. For this we again use the *escape kinetic energy to potential* relation through the escape velocity procedure:

$$\frac{1}{2}v_{\text{rad,eff}}^2(r, Hz) = -\frac{V_{\text{eff}}(r, Hz)}{m} \quad \Rightarrow \quad \frac{V_{\text{eff}}(r, Hz)}{m} = -\frac{1}{2}\left(v_{\text{rad}}(r) - H_z r\right)^2$$

The final result is:

$$\frac{V_{\text{eff}}(r, Hz)}{m} = -\frac{1}{2}\left(\sqrt{\frac{GM}{R}\left(3 - \frac{r^2}{R^2}\right)} - H_z r\right)^2 = \frac{1}{2}v_{rad,eff}^2(r, Hz)$$

so we also have

$$v_{rad,eff}^2(r, Hz) = \left(\sqrt{\frac{GM}{R}\left(3 - \frac{r^2}{R^2}\right)} - H_z r\right)^2.$$

From this we can arrive at the bulge-disk boundary condition, for which we set $r = R$, as:

$$\frac{V_{\text{eff}}(r, Hz)}{m} = -\frac{1}{2}\left(\sqrt{\frac{2GM}{R}} - H_z R\right)^2 = \frac{1}{2}v_{rad,eff}^2(R, Hz)$$

so

$$v_{rad,eff}^2(R, Hz) = \left(\sqrt{\frac{2GM}{R}} - RH_z\right)^2.$$

And for $r = 0$, we get

$$v_{rad,eff}^2(0, Hz) = \frac{3GM}{R} = \frac{3}{2}v_{esc}^2.$$

B. Effective Potential for $r \geq R$, the disk

We define outer effective potential per unit mass in the same way through the intermediary of the velocities of space::

$$\frac{V_{\text{eff}}(r,Hz)}{m} = -\frac{1}{2}\left(v_{esc} - v_H\right)^2 = -\frac{1}{2}\left(\sqrt{\frac{2GM}{r}} - H_z r\right)^2$$

which at $r = R$ can be valuated as:

$$\frac{V_{\text{eff}}(R,Hz)}{m} = -\frac{1}{2}\left(\sqrt{\frac{2GM}{R}} - H_z R\right)^2$$

and gives the same result as the inner effective potential energy. We define $r_c = r$ as the distance at which $v_{esc} = v_H$, so where $V_{eff} = 0$.

C. The Virial Theorem applied to the efffective potential energy at the bulge-disk boundary

We use the virial theorem at $r = R$ for a circular orbit in an effective potential and use it for the metric instead of material particles and we only use it at the boundary between bulge and disk:

$$K_{orb} = -\frac{1}{2}V_{\text{eff}}(R) \quad \Rightarrow \quad \frac{1}{2}mv_{\text{orb}}^2 = -\frac{1}{2}V_{\text{eff}}(R) \quad \Rightarrow \quad v_{\text{orb}}^2 = -\frac{V_{\text{eff}}(R)}{m}$$

From the outside in, we arrive at R from above We use the earlier expression for the effective potential outside the bulge:

$$\frac{V_{\text{eff}}(R)}{m} = -\frac{1}{2}\left(\sqrt{\frac{2GM}{R}} - H_z R\right)^2$$

so

$$v_{orb}^2 = -\frac{V_{\text{eff}}(R)}{m} = \frac{1}{2}\left(\sqrt{\frac{2GM}{R}} - H_z R\right)^2$$

We recall the Lagrangian definition to be:

$$L = K_{orb} - V_{\text{eff}} = \frac{1}{2}mv_{\text{orb}}^2 - V_{\text{eff}}(R)$$

We now substitute $v_{\text{orb}}^2 = -\frac{V_{\text{eff}}(R)}{m}$:

$$L = \frac{1}{2}m\left(-\frac{V_{\text{eff}}(R)}{m}\right) - V_{\text{eff}}(R) = -\frac{1}{2}V_{\text{eff}}(R) - V_{\text{eff}}(R) = -\frac{3}{2}V_{\text{eff}}(R)$$

In short, we have

$$L(R,Hz) = -\frac{3}{2}V_{\text{eff}}(R)$$

We use the earlier expression for the effective potential:

$$\frac{V_{\text{eff}}(R)}{m} = -\frac{1}{2}\left(\sqrt{\frac{2GM}{R}} - H_z R\right)^2$$

in terms of the velocity of space, the square of the Lagrangian velocity becomes:

$$\frac{2L}{m} = v_L^2 = -3\cdot\left(\frac{V_{\text{eff}}(R)}{m}\right) = -3\cdot\left[-\frac{1}{2}\left(\sqrt{\frac{2GM}{R}} - H_z R\right)^2\right] = \frac{3}{2}\left(\sqrt{\frac{2GM}{R}} - H_z R\right)^2$$

This gives the new Lagrangian velocity at R, assuming:

- The orbit at $r = R$ is virialized with respect to the effective potential V_{eff},
- The standard definition $L = K - V$ holds at R.

D. The orbital velocity and Lagrangian inside the bulge

In a previous version of the galactic rotation curves, I constructed a model galaxy with a model bulge with mass M and radius R and an empty space around it [1]. In such a mode galaxy, the Newtonian gravitational potential was fully determined by the bulge. The model bulge has constant density $\rho_0 = \frac{M}{V} = \frac{3M}{4\pi R^3}$ and its composing stars rotate on geodetics in a quasi-solid way. So all those stars in the bulge have equal angular velocity ω on their geodetic orbits, with $v_{orbit} = \omega r$. So we had $v_{orbit}^2 = \omega^2 r^2$ and

$$\frac{K_{orbit}}{m} = \frac{\omega^2 r^2}{2} \tag{1}$$

On the boundary between the quasi solid spherical bulge and the emptiness outside of it, the orbital velocities are behaving smoothly. So the last star in the bulge and the first star in the region outside of the bulge have equal velocities and potentials. We now apply the effective potential. This allows us to determine ω as in

$$\omega_{orb}^2 = \frac{v_{orb}^2(R)}{R^2} = -\frac{V_{\text{eff}}(R)}{mR^2} = \frac{1}{2R^2}\left(\sqrt{\frac{2GM}{R}} - H_z R\right)^2$$

So we get

$$v_{orb}^2(r) = \omega_{orb}^2 r^2 = \frac{v_{orb}^2(R)r^2}{R^2} = -\frac{V_{\text{eff}}(R)r^2}{mR^2} = \frac{1}{2}\left(\sqrt{\frac{2GM}{R}} - H_z R\right)^2 \frac{r^2}{R^2}$$

We can then determine $L(r)$ inside the bulge because $L(r) = K_{orb}(r) + K_{rad,eff}(r)$, so

$$\frac{2L}{m}(r) = v_{orb}^2(r) + v_{rad,eff}^2(r) = \frac{1}{2}\left(\sqrt{\frac{2GM}{R}} - H_z R\right)^2 \frac{r^2}{R^2} + \left(\sqrt{\frac{GM}{R}\left(3 - \frac{r^2}{R^2}\right)} - H_z r\right)^2 .$$

As a result, inside such a model bulge, L is a not constant of the motion of the metric any more.

E. Orbital Velocity for $r > R$

We again postulate that the Lagrangian is constant in the whole disk. For $r > R$, the effective potential is:

$$\frac{V_{\text{eff}}(r)}{m} = -\frac{1}{2}\left(\sqrt{\frac{2GM}{r}} - H_z r\right)^2$$

We define the Lagrangian per unit mass outside the bulge as:

$$\frac{L}{m} = \frac{K_{orb}}{m} + \frac{K_{rad,eff}}{m} = \frac{1}{2}v_{\text{orb}}^2 + \frac{1}{2}\left(\sqrt{\frac{2GM}{r}} - H_z r\right)^2$$

Substitute the conserved value of $\frac{L}{m}$:

$$\frac{1}{2}v_{\text{orb}}^2 + \frac{1}{2}\left(\sqrt{\frac{2GM}{r}} - H_z r\right)^2 = \frac{3}{4}\left(\sqrt{\frac{2GM}{R}} - H_z R\right)^2$$

Solve for v_{orb}^2:

$$v_{orb}^2 = \frac{3}{2}\left(\sqrt{\frac{2GM}{R}} - H_z R\right)^2 - \left(\sqrt{\frac{2GM}{r}} - H_z r\right)^2 .$$

In brief, we have

$$v_{\text{orb}}^2 = \frac{3}{2}v_{rad,eff}^2(R) - v_{rad,eff}^2(r).$$

And for $v_{final,eff} = v_L$ we get

$$v_{\text{final, eff}}^2 = \frac{3}{2}v_{rad,eff}^2(R) = \frac{3}{2}\left(\sqrt{\frac{2GM}{R}} - H_z R\right)^2$$

F. Summary of results

1. The effective values inside *the bulge*

$$v_{orb}^2(r) = \frac{1}{2}\left(\sqrt{\frac{2GM}{R}} - H_z R\right)^2 \frac{r^2}{R^2}$$

$$v_{rad,eff}^2(r,Hz) = \left(\sqrt{\frac{GM}{R}\left(3-\frac{r^2}{R^2}\right)} - H_z r\right)^2 .$$

$$v_L^2(r) = \frac{1}{2}\left(\sqrt{\frac{2GM}{R}} - H_z R\right)^2 \frac{r^2}{R^2} + \left(\sqrt{\frac{GM}{R}\left(3-\frac{r^2}{R^2}\right)} - H_z r\right)^2 .$$

2. *The effective values* outside *the bulge*

$$v_{orb}^2 = \frac{3}{2}\left(\sqrt{\frac{2GM}{R}} - H_z R\right)^2 - \left(\sqrt{\frac{2GM}{r}} - H_z r\right)^2 .$$

$$v_{rad,eff}^2 = \left(\sqrt{\frac{2GM}{r}} - H_z r\right)^2 .$$

$$v_L^2 = v_{final}^2 = \frac{3}{2}\left(\sqrt{\frac{2GM}{R}} - H_z R\right)^2$$

3. *The new spiral pitch angle outside the bulge*

We have

$$\vec{v}_L = \vec{v}_{orb} + \vec{v}_{rad,eff}$$

with

$$\vec{v}_{rad,eff} = -v_{rad,eff}\hat{r} = -\left(\sqrt{\frac{2GM}{r}} - H_z r\right)\hat{r}$$

and

$$\vec{v}_{orb} = v_{orb}\hat{\varphi} = \sqrt{\left(\frac{3}{2}\left(\sqrt{\frac{2GM}{R}} - H_z R\right)^2 - \left(\sqrt{\frac{2GM}{r}} - H_z r\right)\right)}\hat{\varphi}$$

so

$$tan(\alpha_L) = \frac{|v_{rad,eff}|}{|v_{orb}|} = \frac{\sqrt{\frac{2GM}{r}} - H_z r}{\sqrt{\left[\frac{3}{2}\left(\sqrt{\frac{2GM}{R}} - H_z R\right)^2 - \left(\sqrt{\frac{2GM}{r}} - H_z r\right)^2\right]}}$$

and

$$v_L^2 = v_{orb}^2 + v_{rad,eff}^2$$

In appendix (**??**), we plotted spirals for a standard bulge at different z and we included a graph of r_c against cosmic time.

4. New formulas for rotation curve fitting:

Inside the bulge:

$$v_{orb}^2(r) = \frac{1}{2}\left(\sqrt{\frac{2GM}{R}} - H_z R\right)^2 \frac{r^2}{R^2}$$

and ousid the bulge:

$$v_{orb}^2 = \frac{3}{2}\left(\sqrt{\frac{2GM}{R}} - H_z R\right)^2 - \left(\sqrt{\frac{2GM}{r}} - H_z r\right)^2 .$$

5. Specific Lagrangian inside and outside the bulge

In Fig. 1 we present the specific Lagrangian L/m as a function of radius r, separated into its orbital and radial effective contributions. For radii $r \leq R$ the expressions follow directly from the Lagrangian formulation in Eq. (X), where the quadratic terms in $v_{\rm orb}$ and $v_{\rm rad,eff}$ combine to produce the Lagrangian density. For radii $r > R$ the continuation is given by the effective outside–bulge relations [Eqs. (II F 2)–(X)], in which the orbital and radial terms exchange roles while the total value remains a constant $L/m = \frac{1}{2}v_L^2$. This asymptotic constant is split by construction between the orbital and radial channels. The figure further highlights the horizontal fractions $\frac{1}{3}L/m$ and $\frac{2}{3}L/m$, which provide natural reference levels for the partitioning of the constant value in the exterior domain. The vertical dashed line marks $r = R$, i.e. the bulge boundary. The shaded region indicates the continuation to radii $r > R$.

In order to assess how the balance between orbital and radial effective contributions evolves with redshift and stellar mass, we also evaluated the model for intermediate parameters, namely $M = 5 \times 10^8\, M_\odot$ at $z = 1$ with the same bulge radius $R = 2$ kpc. Here the Hubble rate is $H(z{=}1) = 123\,\mathrm{km\,s^{-1}\,Mpc^{-1}}$, corresponding to $0.123\,\mathrm{km\,s^{-1}\,kpc^{-1}}$. Figure 2 compares the resulting specific Lagrangian and contributions with the baseline case ($M = 10^9\, M_\odot$, $H_0 = 70\,\mathrm{km\,s^{-1}\,Mpc^{-1}}$, $R = 2$ kpc). The asymptotic values are reduced from $\simeq 3.2 \times 10^3$ (km/s)^2 in the baseline to $\simeq 1.6 \times 10^3$ (km/s)^2 at $z = 1$, so both curves remain visible on the same vertical scale. This illustrates that for realistic cosmological values the interior partitioning of the Lagrangian remains qualitatively unchanged, but the overall scale shifts systematically with mass and Hubble parameter.

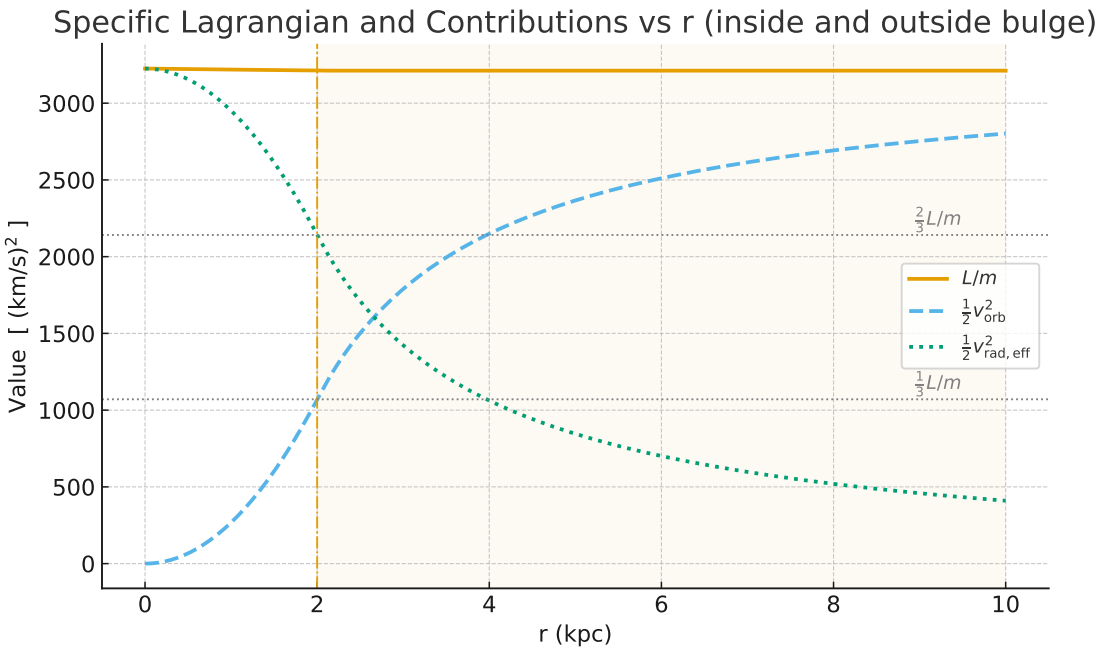

FIG. 1. Specific Lagrangian L/m and its orbital (dashed) and radial effective (dotted) contributions as a function of radius r. The inner solution is shown for $0 \le r \le R$, while the shaded region denotes the outer continuation $r > R$. Horizontal dotted lines mark $\frac{1}{3}L/m$ and $\frac{2}{3}L/m$. Parameters used are $R = 2\,\mathrm{kpc}$, $M = 10^9\,M_\odot$, and $H_z = H_0 = 70\,\mathrm{km\,s^{-1}\,Mpc^{-1}}$.

III. BULGE MASS, ASYMPTOTIC LAGRANGIAN, AND CRITICAL RADIUS AS FUNCTIONS OF REDSHIFT

In order to quantify the interplay between galaxy-internal growth and the cosmological background, we traced the redshift evolution of the bulge mass $M_{\mathrm{bulge}}(z)$, the asymptotic specific Lagrangian $L/m|_\infty$, and the critical radius r_c defined by the balance between gravity and the Hubble expansion. In all cases we adopt a fiducial bulge radius of $R = 2$ kpc and normalize the bulge mass to $M_{\mathrm{bulge}}(z{=}0) = 10^{10}\,M_\odot$.

A. Bulge mass evolution

We parameterize $M_{\mathrm{bulge}}(z)$ with a two-channel model in which $\sim$60% of the final mass is built in situ around the cosmic star formation peak ($z \sim 2$) and the remainder accrues ex situ through mergers toward lower redshift. This parameterization yields a steep rise in mass between $z \sim 6$ and $z \sim 1$ and a flattening thereafter. Figure 3 illustrates this track.

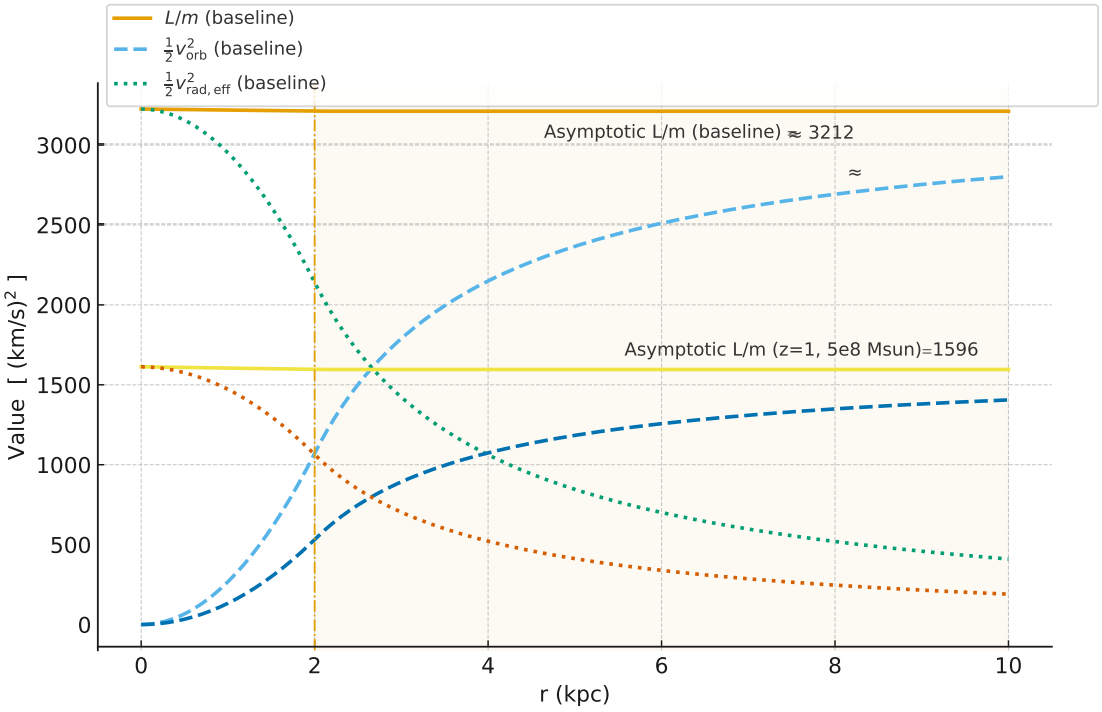

FIG. 2. Comparison of the specific Lagrangian L/m and its orbital (dashed) and radial effective (dotted) contributions as a function of radius r for the baseline parameters ($M = 10^9\,M_\odot$, $H_0 = 70\,\mathrm{km\,s^{-1}\,Mpc^{-1}}$, $R = 2$ kpc) and for the $z = 1$ case ($M = 5\times10^8\,M_\odot$, $H(z{=}1) = 123\,\mathrm{km\,s^{-1}\,Mpc^{-1}}$, $R = 2$ kpc). The shaded region denotes the outer continuation $r > R$. The asymptotic values are $\simeq 3210$ (km/s)^2 (baseline) and $\simeq 1590$ (km/s)^2 ($z = 1$ case).

B. Asymptotic Lagrangian scaling

The asymptotic value of the specific Lagrangian is

$$\left.\frac{L}{m}\right|_\infty(z) \;=\; \tfrac{3}{4}\left(\sqrt{\frac{2GM_{\mathrm{bulge}}(z)}{R}} - H(z)R\right)^2 . \tag{2}$$

For the adopted bulge masses and $R = 2$ kpc, the gravitational term $\sqrt{2GM/R}$ is tens to hundreds of $\mathrm{km\,s^{-1}}$, whereas the Hubble term $H(z)R$ remains of order a few $\mathrm{km\,s^{-1}}$ even at $z = 10$. As a result, $L/m|_\infty$ is governed almost entirely by the bulge mass, with $H(z)$ providing only a percent-level correction. This is evident in Fig. 3, where the redshift dependence of $L/m|_\infty$ directly tracks the growth of $M_{\mathrm{bulge}}(z)$.

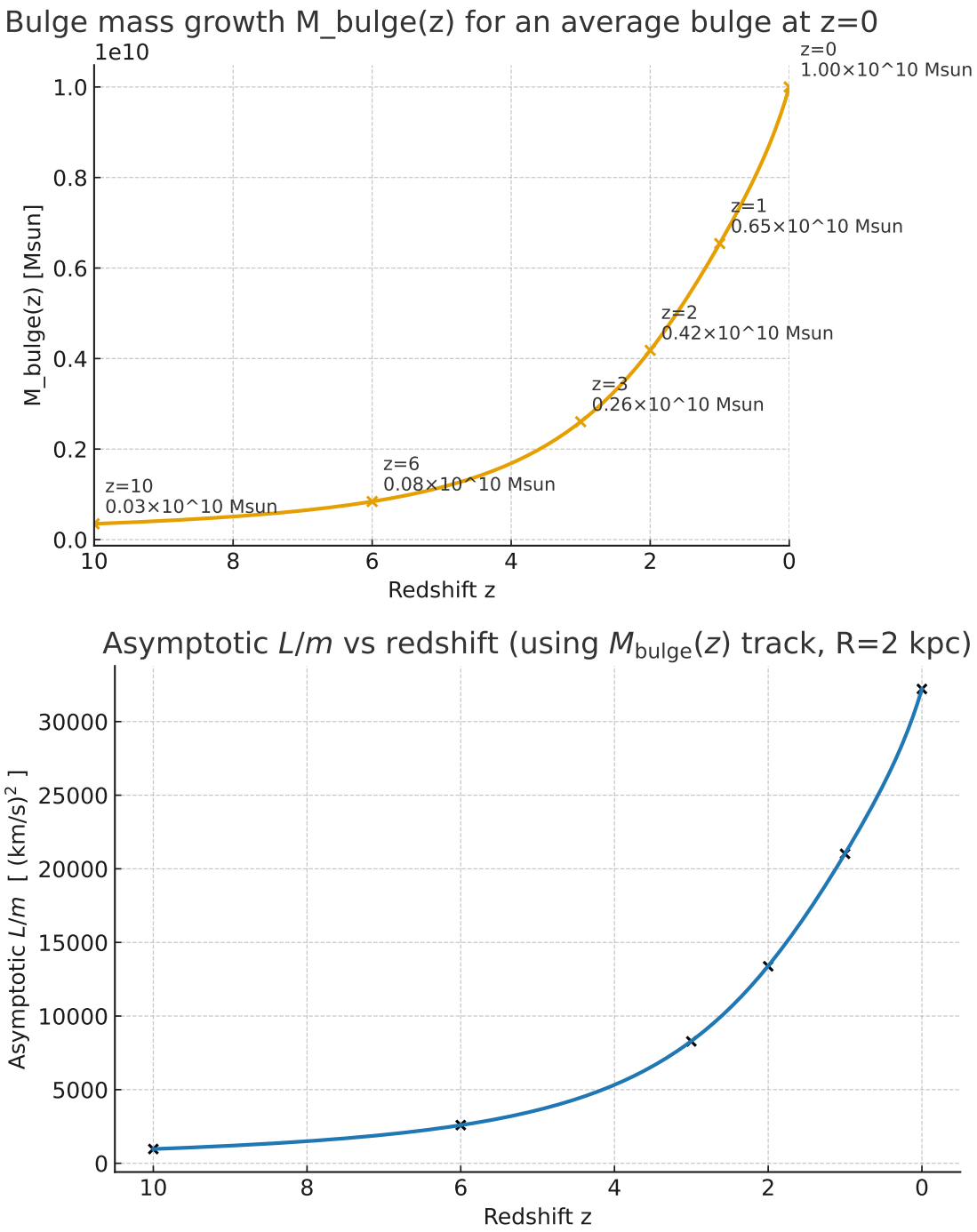

FIG. 3. **Top:** Bulge mass evolution $M_{\rm bulge}(z)$ normalized to $M_{\rm bulge}(z{=}0) = 10^{10}\,M_\odot$ with $R = 2$ kpc. Markers denote selected redshifts $z = 0, 1, 2, 3, 6, 10$. **Bottom:**Asymptotic L/m (blue, left axis) versus redshift for $R = 2$ kpc. The close correspondence with the previous graph of $M(z)$ demonstrates that L/m evolution is mass-driven, with negligible dependence on $H(z)$.

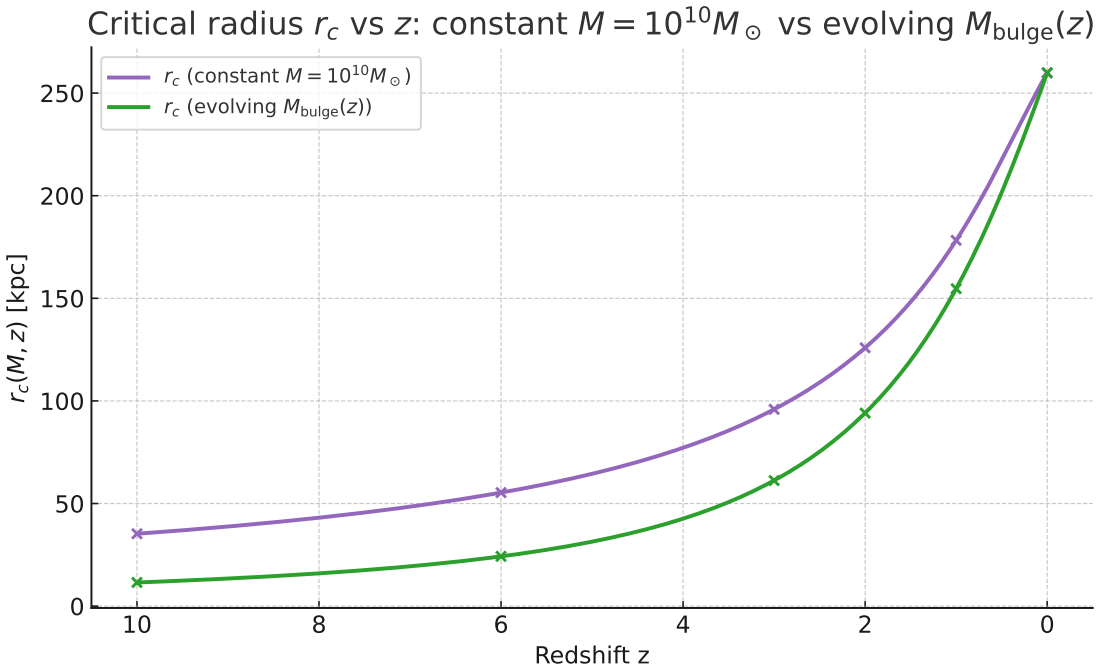

FIG. 4. Critical radius $r_c(M,z)$ as function of redshift. Green: evolving $M_{\rm bulge}(z)$; purple: constant $M = 10^{10} M_\odot$. The strong downward trend with z reflects the dominant $H(z)$ dependence; the difference between the two curves shows the weaker role of $M(z)$.

C. Critical radius scaling

The critical radius is defined by

$$r_c(M,z) = \left(\frac{2GM}{H(z)^2}\right)^{1/3}. \tag{3}$$

Unlike $L/m|_\infty$, here the Hubble rate enters with a strong exponent, $r_c \propto H(z)^{-2/3}$. Across $z = 10$ to $z = 0$, $H(z)$ decreases by roughly a factor of twenty, driving an order-of-magnitude increase in r_c. Mass growth contributes more weakly, as $r_c \propto M^{1/3}$: a thirty-fold bulge mass increase corresponds to only a factor $\sim$3 rise in r_c. Consequently, the overall evolution of $r_c(z)$ is dominated by cosmology rather than bulge mass. Figure 4 compares the critical radius for the evolving $M_{\rm bulge}(z)$ track to the constant-mass case $M = 10^{10} M_\odot$, highlighting the relative contributions.

TABLE I. Scaling of dynamical quantities with bulge mass M and Hubble rate $H(z)$ for fixed $R = 2$ kpc.

Quantity	Dependence on M	Dependence on $H(z)$
Asymptotic L/m	$\propto M$	weak, $\sim -2\sqrt{GM}\,H(z)R$ correction
Critical radius r_c	$\propto M^{1/3}$	$\propto H(z)^{-2/3}$

D. Summary

The relative impact of bulge mass and Hubble expansion on the two quantities of interest is summarized in Table I. For bulges of realistic galactic mass scale ($M \gtrsim 10^8 M_\odot$) at $R = 2$ kpc, the asymptotic Lagrangian evolution is predominantly mass-driven, while the critical radius evolution is cosmology-driven. This separation of roles clarifies the relative impact of galactic growth versus the Hubble flow in shaping the dynamical scales. For rotation curves, this implies that the impact of Hz on the size of v^2_{final} is in the few percentage range. But the impact of higher Hz, through its impact on r_c, should be observable as a faster approach of v^2_{orb} towards the asymptotic $v^2_{final} = v^2_L$. And the shape of spirals should also be impacted by the evolution of r_c because a smaller r_c squeezes the spiral inwards and forces its faster towards the final circle at r_c.

IV. DYNAMICS OF ROTATION CURVES AND SPIRAL ARMS IN THE CONSTANT LAGRANGIAN METRIC APPROACH

In previous work, I developed a new theory of galactic spiral dynamics based on a constant metric Lagrangian [2]. This work was a continuation of my work on galactic rotation curves [1], were I fitted galaxy rotation curves on the constant Lagrangian curve. These works had the velocity of space theory of gravity as background, a metric theory of gravity that had one of its foundations in Hubble space expansion, as I elaborated earlier, see [3] and the references therein. I then realized that the combination of these works led to a new way to determine the Hubble parameter from galactic spiral morphology. Notably, the shape of the spiral depends sensitively on H_z, which opens the possibility of using spiral morphology as direct cosmological probes.

But eventually the rotation curve's Hz sensitivity might also become a way to determine Hz from rotation curves. Given a galaxy with a well-measured rotation curve $v_{\rm obs}(r)$, and a reasonable estimate of the central bulge mass M and reference radius R from stellar light or kinematics, one can numerically invert Eq. (II F 2) to fit for the value of H_z that best reproduces the observed

curve. Reasonable means determining R and M with measurement errors of at most a few percentage. This approach would then allow one to empirically derive the Hubble parameter $H(z)$ from individual galaxies, independent of standard cosmological assumptions. The rotation curve method offers potenntial direct extraction of H_z from galaxy dynamics, with a high statistical potential of thousands to millions of spiral galaxies with usable data. It is applicability across a broad redshift range ($z = 0$ to $z \sim 6$). Thus, rotation curves could serve, in the future, not only as diagnostic tools for galactic structure but also as precision probes of cosmological expansion within the metric inflow paradigm.

V. TRACING SPIRAL MORPHOLOGY BACKWARDS IN TIME

A. Mass dependence of spiral morphology at $z \approx 0$

For nearby galaxies ($z \simeq 0$) the Hubble rate is nearly constant and the bulge radius R can be treated as fixed on galactic scales. In this regime the only remaining free parameter controlling the morphology of the inflow spirals is the bulge mass M. To isolate this dependence, we computed dual–arm solutions for $R = 2$ kpc and four different masses, $M = 10^7$, 10^8, 10^9, and $10^{10} M_\odot$, truncated at $r = 20$ kpc. The integration employed the local Hubble parameter $H(z{=}0) = 0.07$ km s^{-1} kpc^{-1}.

Figure 5 shows the resulting spiral loci in the (x, y) plane. At the lowest mass ($M = 10^7 M_\odot$) the arms remain tightly wound near the bulge, with small pitch angles. As the mass increases, the stronger gravitational potential steepens the orbital component and opens the spiral morphology. By $M = 10^{10} M_\odot$ the arms extend rapidly to large radii, producing a much more open two–armed pattern. Thus, in the local universe the bulge mass alone sets the geometry of the inflow spiral, while cosmological effects encoded in $H(z)$ are negligible.

B. Redshift dependence of inflow spirals

To illustrate the evolution of inflow patterns over cosmic time we computed the single–arm spirals for bulges of fixed physical radius $R = 2$ kpc at redshifts $z = 0$, 2, 3, and 6. The bulge mass at each epoch was taken from the fiducial mass–growth track normalized to $M_{\rm bulge}(z{=}0) = 10^{10} M_\odot$. This yields masses $M(z{=}0) = 1.0 \times 10^{10} M_\odot$, $M(z{=}2) = 4.2 \times 10^9 M_\odot$, $M(z{=}3) = 2.6 \times 10^9 M_\odot$,

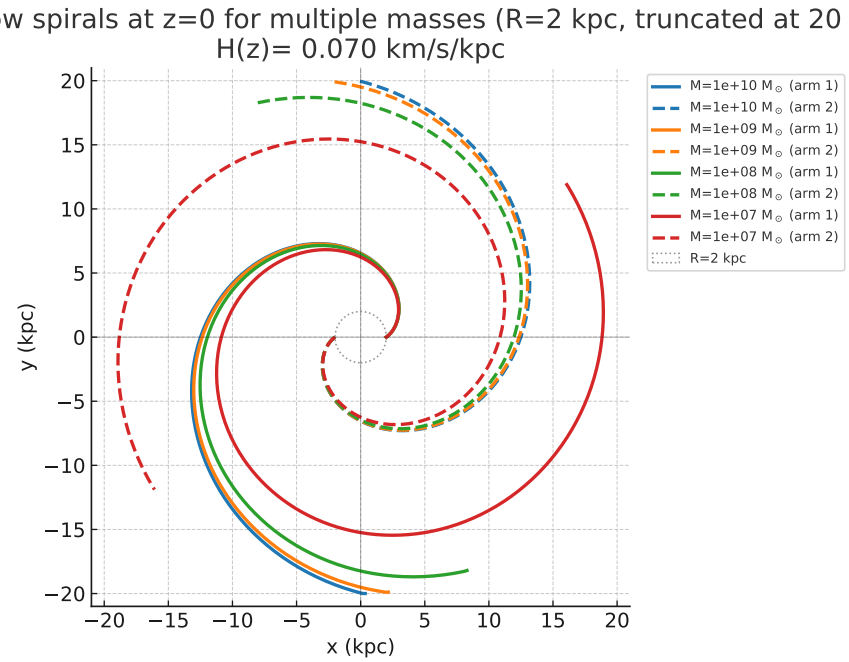

FIG. 5. Dual–arm inflow spirals at $z = 0$ for a fixed radius $R = 2$ kpc and masses $M = 10^7$ (red), 10^8 (green), 10^9 (orange), and $10^{10} M_\odot$ (blue). Dashed curves show the arm rotated by 180°. The arms are integrated out to 20 kpc; the circle marks the bulge radius. With $H(z)$ constant at low redshift, variation in M alone drives the change from tightly wound to widely open spiral geometries.

and $M(z{=}6) = 8.4 \times 10^8 M_\odot$. For each case the critical radius

$$r_c(M(z), H(z)) = \left(\frac{2GM(z)}{H(z)^2} \right)^{1/3} \tag{4}$$

was evaluated using a flat ΛCDM cosmology with $H_0 = 70\ \mathrm{km\,s^{-1}Mpc^{-1}}$, $\Omega_m = 0.3$, $\Omega_\Lambda = 0.7$.

Figure 6 shows the resulting spiral loci in the (x, y) plane together with their r_c circles. The present–day case ($z = 0$) exhibits an extended spiral with $r_c \sim 260$ kpc, while at higher redshift the combination of reduced bulge mass and larger $H(z)$ compresses the pattern to smaller scales ($r_c \simeq 24$ kpc at $z = 6$). Thus the spiral inflow pattern contracts strongly with redshift, tracking the cosmological evolution of $H(z)$ modulated by the concurrent bulge mass growth.

This numerical trend is consistent with the analytic scaling relation $r_c \propto M^{1/3} H(z)^{-2/3}$. Over the interval $z = 0$ to $z = 6$, $H(z)$ increases by nearly an order of magnitude, while $M(z)$ decreases by a factor of ~ 10. The net effect is a contraction of r_c by an order of magnitude, in good agreement with the values shown in the figure. Hence the plotted spirals provide a direct visualization of how the competing dependencies on bulge mass and the Hubble rate shape the inflow geometry.

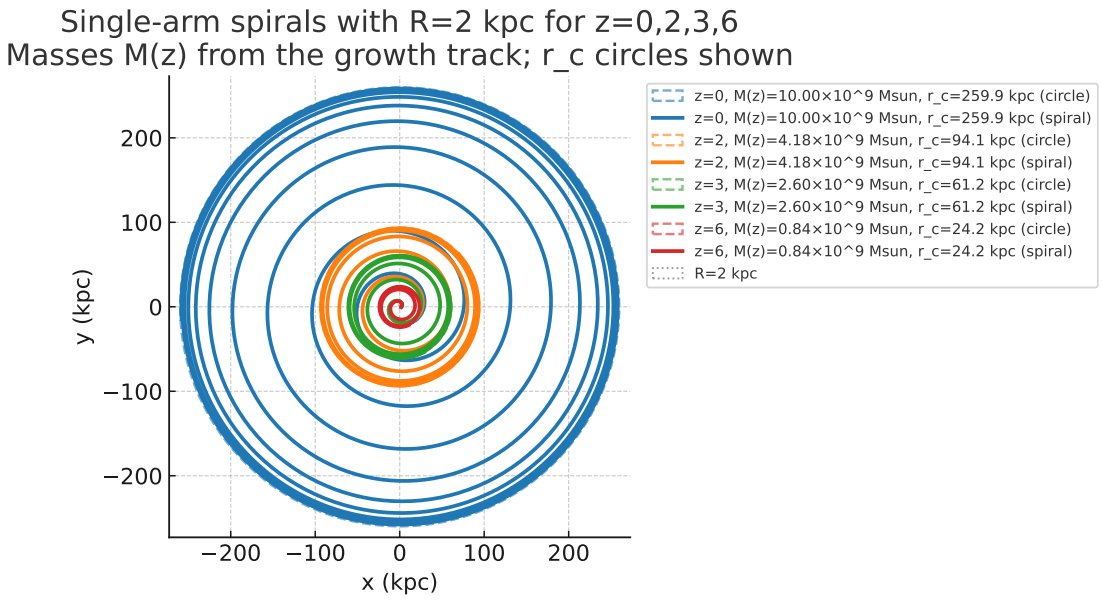

FIG. 6. Single–arm inflow spirals for bulges with fixed $R = 2$ kpc at $z = 0$ (blue), $z = 2$ (orange), $z = 3$ (green), and $z = 6$ (red). Bulge masses $M(z)$ are taken from the fiducial growth track ($M(z{=}0) = 10^{10}\,M_\odot$). Dashed circles mark the corresponding critical radii $r_c(M,z)$, ranging from ~ 260 kpc at $z = 0$ to ~ 24 kpc at $z = 6$.

C. Double–arm inflow spirals at high redshift

To illustrate the morphology of inflow patterns in the early universe, we computed dual–arm spirals (a single solution and its 180° rotation) at redshifts $z = 3$, 10, 15, and 20. The bulge radius R was set to 2 kpc for $z = 3$ and 10, and to 1 kpc for $z = 15$ and 20, while the bulge mass was chosen to match the fiducial growth track at each epoch. The resulting parameters are $M(z{=}3) = 2.6\times10^9\,M_\odot$, $M(z{=}10) = 3.0\times10^8\,M_\odot$, $M(z{=}15) = 1.0\times10^8\,M_\odot$, and $M(z{=}20) = 5.0\times10^7\,M_\odot$.

The spirals were integrated outward from R to the critical radius where the radial inflow velocity vanishes. At $z = 20$ we find $H(z) = 3.69$ km s^{-1}kpc^{-1} and $r_c = 3.16$ kpc, at $z = 15$ we find $H(z) = 2.45$ km s^{-1}kpc^{-1} and $r_c = 5.23$ kpc, at $z = 10$ the pattern extends to $r_c = 10.96$ kpc, and at $z = 3$ the present observational limit for galaxy imaging is reached, with $H(z) = 0.31$ km s^{-1}kpc^{-1} and $r_c = 61.2$ kpc. The figures show both spiral arms, the bulge radius, and the critical radius as dashed and dash–dotted circles.

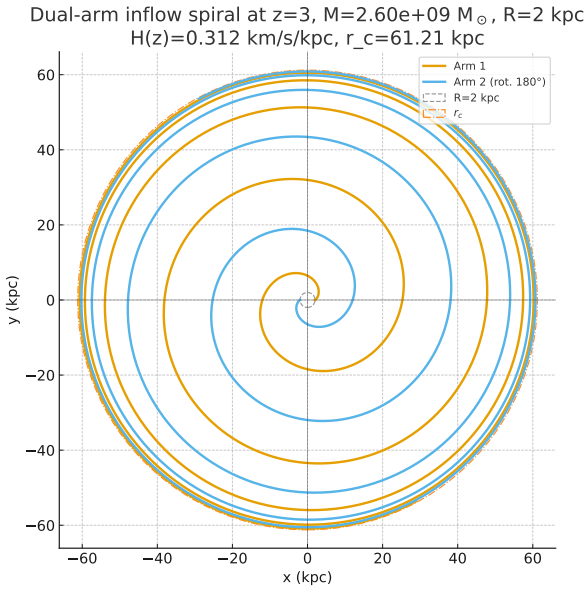

FIG. 7. Dual–arm inflow spiral at $z = 3$ for a bulge of radius $R = 2$ kpc and mass $M = 2.6 \times 10^9 M_\odot$. Both arms are shown, together with the bulge radius (dashed circle) and the critical radius $r_c = 61.2$ kpc (dash–dotted circle). This redshift marks the present observational limit for galaxy imaging, beyond which only theoretical extrapolations of the spiral morphology are currently possible.

VI. NESTED SPIRAL FORMATION FROM METRIC INFLOW AND BULGE RESET EVENTS

Once, in cosmic time, a bulge has developed a small disk, both whith the spiral metric inflow structure, the disk region expands due to two factors:

1. Continuous accretion of gas by the inward-moving metric increases the central mass.

2. The Hubble parameter $H(z)$ decreases, expanding r_c even without additional mass.

This dynamic creates a feedback loop where inflow drives mass growth, which in turn expands the inflow region.

In cases where the mass has been accumulating in the spiral near to the bulge without flowing into the bulge, for example because the mass is orbiting instead of inflowing, the metric can get unstable until a reset of the bulge is realises. A new spiral develops and the old spiral turnes into a nested spiral that can develop into a bar. The morphology of such a galaxy can become complicated, with a bulge-bar-circle-disk structure. If a super massive black hole or SMBH developes

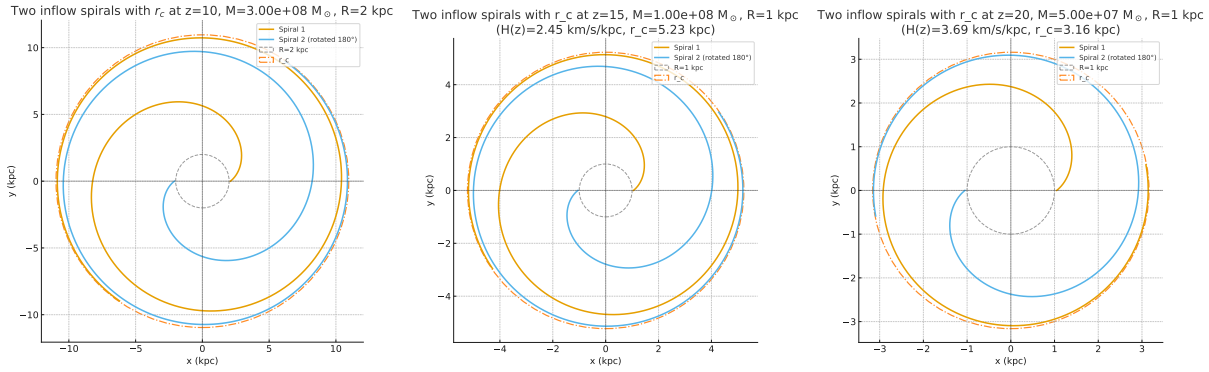

FIG. 8. Double–arm inflow spirals at redshifts $z = 10$, 15, and 20. Bulge radii are $R = 2$ kpc ($z = 10$) and $R = 1$ kpc ($z = 15, 20$). Bulge masses are $M(z{=}10) = 3.0 \times 10^8 M_\odot$, $M(z{=}15) = 1.0 \times 10^8 M_\odot$, and $M(z{=}20) = 5.0 \times 10^7 M_\odot$. Dash–dotted circles indicate the corresponding critical radii $r_c(M, z)$. The opening angle of the arms increases systematically with cosmic time as both $M(z)$ and $H(z)$ evolve.

in the centre of the bulge and an outer gas-dust halo in between spiral disk and critical radius develops, the morphology reads SMBH-bulge-bar-circle-disk-halo.

A. Examples of nested spiral configurations

The feedback process described in Sec. VI can produce galaxies in which two distinct inflow spirals coexist: an older spiral that has expanded to larger radii, and a younger spiral formed after a bulge reset event. In such cases the outer spiral traces the previous inflow morphology, while the newly formed inner spiral develops within the reset bulge region. The result is a nested pattern in which two sets of arms overlap, potentially evolving into bar–like features embedded inside larger disks.

Figure 9 shows an example with an outer spiral representing $z = 3$ ($M = 2.6 \times 10^9 M_\odot$, $R = 3$ kpc) truncated at 15 kpc, and a younger nested spiral at $z = 20$ ($M = 5.0 \times 10^7 M_\odot$, $R = 1$ kpc). The inner structure retains its own critical radius $r_c = 3.16$ kpc, well separated from the larger–scale $z = 3$ pattern.

A second case is shown in Fig. **??**, where the outer spiral corresponds to $z = 0$ ($M = 10^{10} M_\odot$, $R = 3$ kpc) and is truncated at 15 kpc, while the nested inner spiral again represents the $z = 20$ configuration. This illustrates how an early inner spiral can survive as a bar–like or ring–like feature embedded within the much more extended present–day spiral structure.

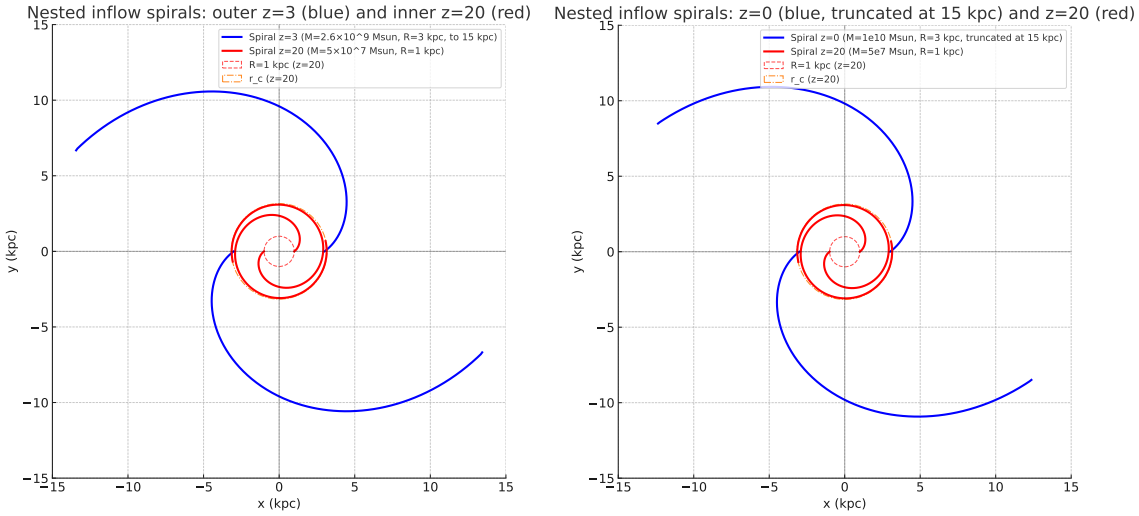

FIG. 9. **Left:**Nested inflow spirals: outer $z = 3$ (blue, truncated at 15 kpc) and inner $z = 20$ (red). The inner spiral has $M = 5.0 \times 10^7 M_\odot$, $R = 1$ kpc and $r_c = 3.16$ kpc. The coexistence of both structures illustrates how bulge reset events can produce overlapping spiral patterns. **Right:**Nested inflow spirals: outer $z = 0$ (blue, truncated at 15 kpc) and inner $z = 20$ (red).

VII. SPIRAL GEOMETRY AS A COSMOLOGICAL PROBE

In the metric inflow framework, the geometry of spiral structure is not incidental but fundamental. Spiral arms trace the trajectory of spacetime itself, flowing inward under gravity as mass-space-absorption with both radial and azimuthal components. This spiral form is governed by the ratio of the effective radial inflow velocity to the azimuthal orbital velocity of the metric:

$$\tan(\alpha_L(r)) = \frac{|\vec{v}_{\text{rad,eff}}|}{|\vec{v}_{\text{orb}}|} = \frac{\sqrt{\frac{2GM}{r}} - H_z r}{\sqrt{\frac{3}{2}\left(\sqrt{\frac{2GM}{R}} - H_z R\right)^2 - \left(\sqrt{\frac{2GM}{r}} - H_z r\right)^2}}, \tag{5}$$

where M is the mass of the central bulge, R is a reference radius (e.g., bulge radius), and H_z is the Hubble parameter at the time the spiral structure is observed or, in the case of nested spirals, became nested.

Given this relationship, one can treat the observed pitch angle $\alpha_L(r)$ of a galaxy's spiral arm as a direct probe of the cosmic expansion rate at its time of formation. Specifically:

- From high-resolution imaging, the spiral structure can be extracted and the pitch angle measured as a function of radius.

- With estimates of the central mass M and a known reference radius R, the full right-hand side of Eq. (5) can be inverted numerically to solve for H_z.

- This yields an effective estimate of the Hubble parameter at the epoch when that spiral layer formed.

Furthermore, when this analysis is combined with the galaxy's optical redshift z_{opt}, one can potentially reconstruct the function $H(z)$ empirically—entirely from observed galaxy morphology and spectroscopy. Each spiral structure effectively serves as a timestamped imprint of the metric dynamics that created it.

VIII. FUTURE POTENTIAL VOLUME OF $H(z)$ DATA FROM ROTATION CURVES AND SPIRAL FITS

A major advantage of the gravitational metric inflow model is that observable galactic features—such as spiral structure and rotation curves—can directly encode the Hubble parameter $H(z)$ at the epoch $t(z)$ when the structure is observed or was frozen as a nested spiral. This enables each spiral galaxy to serve as a cosmological chronometer.

In the metric inflow framework, orbital velocity profiles are determined by a balance between gravitational inflow and cosmological expansion. As shown in Eq. (II F 2), the orbital velocity at radius r depends on the central mass M, the bulge radius R, and the Hubble parameter H_z. Fitting observed rotation curves with this model allows extraction of an effective $H(z)$ at the time the rotation pattern was established.

Similarly, the pitch angle of spiral arms, measurable from high-resolution imaging can be inverted to yield $H(z)$ using the metric inflow velocity equations. Multiple spiral layers in a galaxy may correspond to successive epochs of structure formation, enabling multi-redshift $H(z)$ measurements from a single object. Table II compares the potential number of $H(z)$ points that can be extracted from current and future methods.

IX. CONCLUSION

We have shown that the inclusion of the Hubble parameter $H(z)$ in the Newtonian framework naturally produces limits on the reach of gravitation, leading to a critical radius that evolves with

TABLE II. Estimated number of $H(z)$ data points obtainable from various methods.

Method	Estimated Data Points	Redshift Range	Source/Comments
BAO (standard)	20–30	$0.1 < z < 2.3$	SDSS, eBOSS, DESI
Cosmic chronometers	$\sim$30	$0.1 < z < 2.0$	Galaxy spectra
Strong lensing delays	$\sim$5	$0.5 < z < 2.5$	Quasar lenses
CMB model fit	1	$z \approx 1100$	Planck
Rotation curves (this work)	10,000–100,000	$z = 0.01$–1.5	HI + optical kinematics
Spiral fits (this work)	100,000–1,000,000	$z = 0.01$–6	Optical imaging morphology

cosmic time. This approach connects galactic rotation curves, spiral morphology, and bulge formation to the cosmic expansion in a direct and testable way. The analysis suggests that galactic bars are fossil records of high-z epochs frozen into present-day galaxies, with compact spirals nested in extended structures formed at later times. In this picture the morphology of galaxies becomes a tracer of cosmic history, offering an alternative route to determine the Hubble parameter $H(z)$ from local observations.

The proposed framework therefore provides a new perspective on the Hubble parameter: one may attempt to measure $H(z)$ directly from galactic dynamics and morphology. By systematically applying the method to large galaxy samples across a range of redshifts, it becomes possible to empirically reconstruct the expansion history of the universe and to test the consistency of cosmological models on galactic scales.

REFERENCES

[1]de Haas, E. P. J. (2018). A 'constant lagrangian' rmw-rss quantified fit of the galaxy rotation curves of the complete sparc database of 175 ltg galaxies. *viXra.org:Astrophysics*, page https://vixra.org/abs/1908.0222.

[2]de Haas, E. P. J. (2025a). One single metric model's unifying perspective on four issues with galactic dynamics: B-tf relation, rotation curves, spirals and smbh-growth. *viXra:2506.0097*. preprint https://vixra.org/abs/2506.0097.

[3]de Haas, E. P. J. (2025b). Space quantum gravity. *Journal of High Energy Physics, Gravitation and Cosmology*, 11(2).